communications biology

Article

https://doi.org/10.1038/s42003-024-06679-4

Calorie restriction and rapamycin distinctly mitigate aging-associated protein phosphorylation changes in mouse muscles

Meric Ataman [1,2,5] ✉, Nitish Mittal [1,5], Lionel Tintignac [3], Alexander Schmidt [1], Daniel J. Ham [1], Asier González [1,4], Markus A. Ruegg [1] & Mihaela Zavolan [1,2] ✉

Calorie restriction (CR) and treatment with rapamycin (RM), an inhibitor of the mTORC1 growth-promoting signaling pathway, are known to slow aging and promote health from worms to humans. At the transcriptome and proteome levels, long-term CR and RM treatments have partially overlapping effects, while their impact on protein phosphorylation within cellular signaling pathways have not been compared. Here we measured the phosphoproteomes of *soleus*, *tibialis anterior*, *triceps brachii* and *gastrocnemius* muscles from adult (10 months) and 30-month-old (aged) mice receiving either a control, a calorie restricted or an RM containing diet from 15 months of age. We reproducibly detected and extensively analyzed a total of 6960 phosphosites, 1415 of which are not represented in standard repositories. We reveal the effect of these interventions on known mTORC1 pathway substrates, with CR displaying greater between-muscle variation than RM. Overall, CR and RM have largely consistent, but quantitatively distinct long-term effects on the phosphoproteome, mitigating age-related changes to different degrees. Our data expands the catalog of protein phosphorylation sites in the mouse, providing important information regarding their tissue-specificity, and revealing the impact of long-term nutrient-sensing pathway inhibition on mouse skeletal muscle.

Aging has been recognized as a risk factor for chronic, inflammatory, and malignant diseases[1]. A major consequence of aging is the loss of muscle strength and mass[2], called sarcopenia. Multiple perturbations have been reported to contribute to sarcopenia, including reduced anabolic signaling, insulin resistance, and chronic inflammation[3]. A key player in muscle proteostasis is the mammalian target of rapamycin (mTOR), a serine/threonine kinase that regulates cell growth in response to nutrients and other signals by promoting anabolic processes and inhibiting catabolic processes such as autophagy[4,5]. mTOR takes part in two structurally and functionally different complexes, mTORC1 and mTORC2[6]. The activity of mTORC1 is elevated in aged mouse muscle[5], and sustained mTORC1 activation results in a severe, late-onset myopathy characterized by impaired autophagy[7]. Conversely, long-term mTORC1 inhibition with rapamycin (RM) preserves muscle mass and function in aged animals. Altogether, these and other studies support the notion that increased mTORC1 activity is a hallmark of sarcopenia[5]. Consistent with mTOR's centrality in many aging-related processes[8], RM and calorie restriction (CR) represent the most robust and promising interventions to delay aging and age-related diseases. Both of these treatments improve muscle functionality in aged mice, but their efficacy varies strongly between the muscles that were analyzed, specifically *soleus*, *tibialis anterior*, *triceps brachii*, and *gastrocnemius*[9]. Furthermore, the molecular underpinnings of these functional responses are insufficiently understood, as prior investigations were limited to the mRNA-level responses of the muscles to the treatments. To fill this gap, we here measured the impact of aging (AGE), RM, and CR on signaling via protein phosphorylation in the same four muscles found before to respond differently to the RM and CR treatments[9]. We measured the phosphopeptide content of these muscles in adult (10 months, 10 M), aged (30 M), and aged

[1]Biozentrum, University of Basel, Basel, Switzerland. [2]Swiss Institute of Bioinformatics, Basel, Switzerland. [3]Department of Neurology and Biomedicine, University of Basel; University Hospital Basel, Basel, Switzerland. [4]Departament de Bioquímica i Biologia Molecular and Institut de Biotecnologia i Biomedicina, Universitat Autònoma de Barcelona, Cerdanyola del Vallès, Spain. [5]These authors contributed equally: Meric Ataman, Nitish Mittal. ✉e-mail: meric.ataman@unibas.ch; mihaela.zavolan@unibas.ch

mice that were either calorie restricted (30M_CR) or treated with RM (30M_RM) from 15 months of age. We detected a total of 6960 phosphosites, 1415 of which are not represented in the PhosphoSitePlus database, the main repository in the field[10–13]. Long-term RM treatment led to an overall reduction in the phosphorylation of many mTORC1 substrates, and the most consistent response was seen in substrates of ribosomal protein S6 kinase beta-1 (Rps6kb), which is itself a key target of mTORC1. We demonstrate that CR and RM have quantitatively distinct long-term effects on the phosphoproteome, mitigating aging-related changes to different degrees and in muscle-dependent manners. Our data expands the catalog of protein phosphorylation sites in the mouse, providing important information regarding their tissue-specificity.

Results

Phosphoproteomes are muscle-specific and partially driven by gene expression

We determined the phosphoproteome of four mouse muscles with diverse anatomical locations and functional properties whose response to aging and long-term CR and RM anti-aging interventions we have previously described[9]. Of the four muscles, *soleus* contains predominantly slow-twitch fibers, while *tibialis anterior, triceps brachii,* and *gastrocnemius*, all primarily contain fast-twitch fibers[9,14] (Fig. 1A). We identified ~7000 non-redundant phosphorylation sites from each muscle (Fig. 1B), with 6780 being detected in all four muscles (Supplementary Data 1). Principal component analysis (PCA) of phosphopeptide signal intensities showed separation of *soleus* samples from the others along the first PC and a less pronounced separation of *tibialis anterior* samples along the second PC. *Triceps* and *gastrocnemius* samples were largely interspersed with each other (Fig. 1C). To determine whether differences in phosphopeptide abundance between muscles coincided with differences in gene expression, we also obtained mass spectrometry-based measurements of total protein levels in these muscles. Indeed, when comparing either *soleus* or *tibialis anterior* muscles with the other muscles, differences in phosphopeptide signal intensities significantly correlated with differences in the protein's abundance, especially for *soleus* (Fig. 1D, E). However, the signal intensities of distinct phosphorylation sites within a given protein varied widely, indicating that protein levels do not fully explain phosphopeptide intensities (Supplementary Data 2). Two examples are myomesin 1 (Myom1) in the *soleus* muscle (Fig. 1F) and actinin alpha 2 (Actn2) in *tibialis anterior* (Fig. 1G). In both cases, protein level is lower than in other muscles, but the specific phosphorylation site in the protein increases.

To identify the biological processes specifically affected in each muscle, we selected phosphopeptides aligning to the PC (absolute z-score ≥ 1.96; correlation ≥ 0.5) that best distinguished each muscle from the others (i.e., PC1 for *soleus*, PC2 for *tibialis anterior*), as we have previously described[5], and submitted the corresponding genes to Gene Ontology over-representation analysis. *Soleus*-specific phosphopeptides come from proteins involved in cytoskeletal organization, muscle development, and calcium sequestration, while *tibialis anterior*-specific phosphopeptides come from proteins involved in mRNA processing and localization

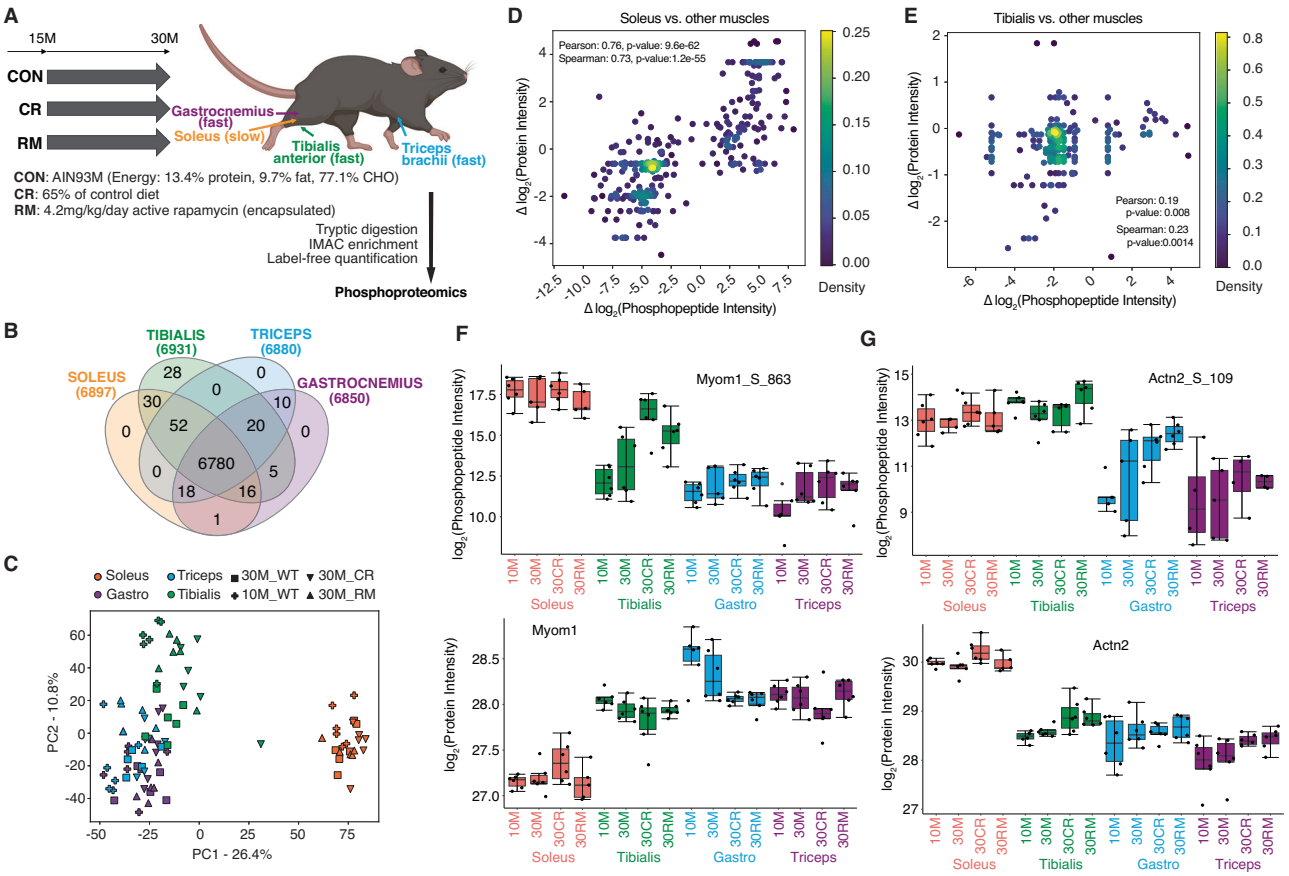

Fig. 1 | Overview of the phosphoproteome data. A Experimental design, mouse image is from Biorender.com. **B** Venn diagram showing the number of phosphosites detected in each muscle (union of all sites identified in samples from a given muscle, irrespective of age and treatment). **C** PCA of the entire data set. Each symbol corresponds to a sample, color indicates the muscle type and symbol the condition. **D** Correlation of changes in the average normalized intensity of 317 phosphopeptides that align with PC1 with changes in corresponding proteins in *soleus* compared to all other muscles. **E** Similar for 119 phosphopeptides in *tibialis anterior*. **F** Example of the S863 phosphosite on Myom1 with a higher intensity in *soleus* than other muscles, despite Myom1 protein levels being lowest in this muscle. **G** S109 phosphorylated Actn2 has a higher intensity in *tibialis anterior* than other muscles, uncorrelated with the protein level. **F**, **G** show boxplots, individual samples being indicated by dots.

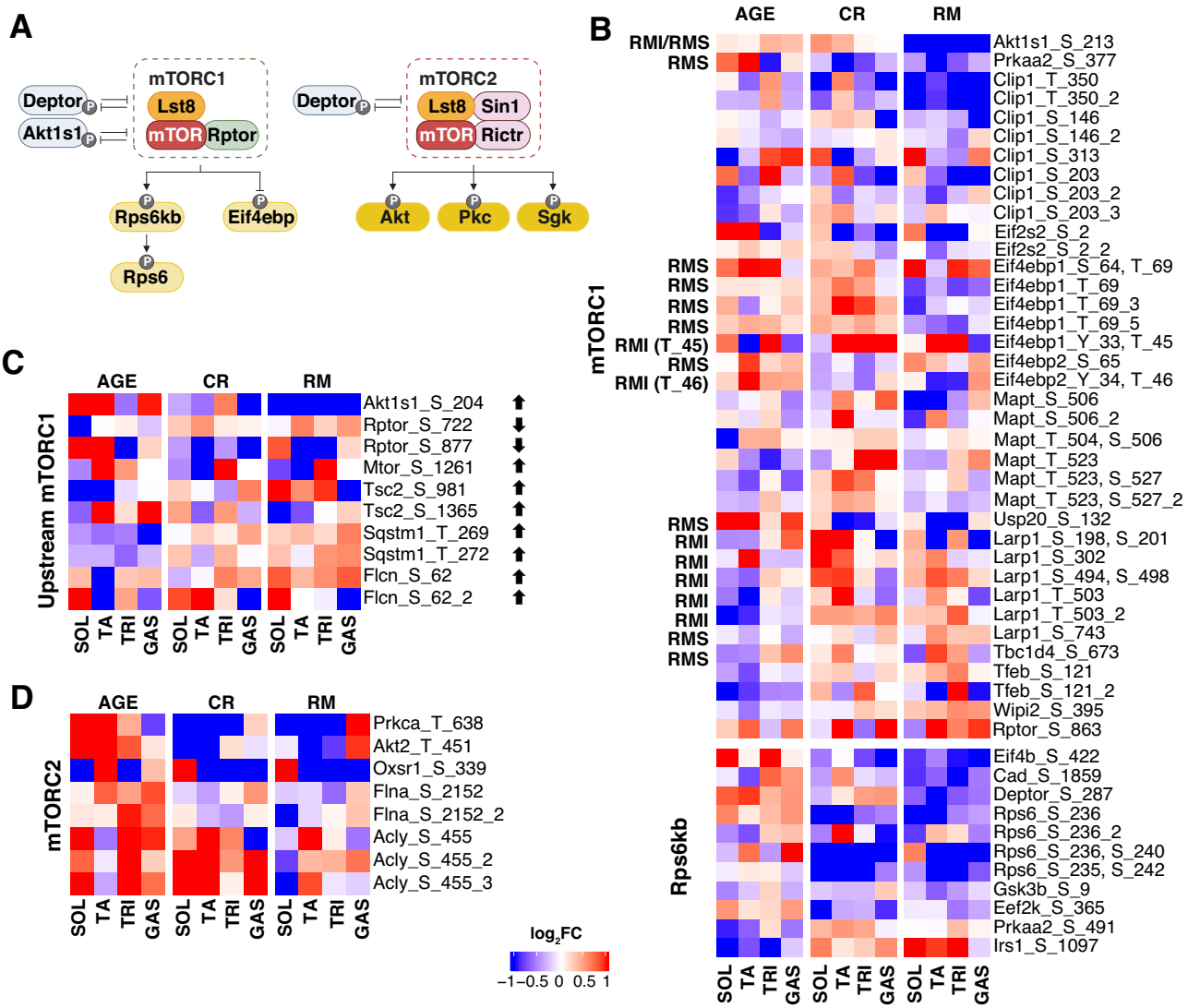

Fig. 2 | AGE, CR, and RM effects on mTOR signaling. A Schematic diagram of mTOR signaling, created with Biorender.com. **B** Phosphosites in direct substrates of mTORC1 and of Rps6kb (see also Supplementary Data 3). Labels on the left indicate that the site has been reported to be RM insensitive (RMI) or sensitive (RMS). Deptor has been shown to be phosphorylated on S287 by casein kinase I isoform alpha (Ck1α)[71,72] and by Rps6kb[73]. We detected 5 phosphosites on Clip1, a protein known to be phosphorylated by mTORC1, at sites so far unmapped[74]. The 4 phosphosites shown here do not have an associated kinase in the PhosphositePlus database. One site (S311 in mouse) has been assigned to 5'-AMP-activated protein kinase (AMPK) and is not shown. **C** Phosphorylation sites in upstream mTORC1 regulators. Black arrows on the right indicate the impact of the site's phosphorylation on mTORC1 (Supplementary Data 3). **D** Phosphorylation sites in direct substrates of mTORC2. If a site has been captured in multiple distinct peptides, these are numbered and reported individually (e.g., "Flcn_S_62_2"). If the peptides contained multiple phosphosites, all of these are reported (e.g., "Eif4ebp1_S_64, T_69").

(Supplementary Fig. 1). Thus, the variation in phosphopeptide intensity is only partially due to the variation in protein abundance between muscles. The *soleus* and *tibialis anterior* muscles can be distinguished from the other two muscles based on phosphopeptide signal intensities, despite most peptides being detected in all four muscles.

Long-term RM treatment broadly reduces phosphorylation of mTORC1 targets

RM is known to acutely inhibit the activity of mTORC1 towards some, but not all substrates, while mTORC2 substrates are relatively resistant to RM[15] (Fig. 2A). To validate our data and better understand the basis of muscle-specific responses to CR and RM[9] we calculated log2 fold changes in peptide intensity between 30M_WT and 10M_WT, 30M_CR or 30M_RM samples for individual muscles, thereby capturing AGE, CR and RM effects, respectively. We then interrogated the behavior of direct mTORC1 and Rps6kb substrates, upstream mTORC1 regulators, and mTORC2 substrates (Supplementary Data 3) in our dataset. We tabulated 62 direct mTORC1 substrates, 56 of which came from Battaglioni et al.[6], while the other six were E3 ubiquitin-protein ligase parkin (Prkn)[16], N-terminal kinase-like protein (Scyl1)[17], serine/threonine-protein kinase 11-interacting protein (Stk11iP)[18], eukaryotic translation initiation factor 4E-binding protein 2 (Eif4ebp2), Eif4ebp3, and Rps6kb2. The 12 direct Rps6kb substrates were taken from Barilari et al.[19].

We were able to detect 25 sites in 12 mTORC1 substrates and 10 sites in 8 Rps6kb substrates (Fig. 2B). The pattern of aging-associated phosphorylation site changes was muscle-dependent, with some sites in the CAP-Gly domain-containing linker protein 1 (Clip1), La-related protein 1 (Larp1) and 5'-AMP-activated protein kinase catalytic subunit alpha-2 (Prkaa2) proteins showing decreased phosphorylation in the *soleus* and *tibialis anterior* muscles, while other sites (Clip1 S313) simultaneously displayed increased phosphorylation in the *triceps* and *gastrocnemius* muscles. These results are in line with the initial clustering of the samples based on signal intensities of all phosphosites measured in all muscles (Fig. 1C). Long-term RM treatment reduced the phosphorylation of the majority of RM-sensitive

mTORC1 substrates, and most consistently reduced the phosphorylation of Rps6kb substrates (including Rps6 as described in ref. 5). In contrast, CR had more variable effects across muscles than RM, and in the case of Eif4ebp1 T69 phosphorylation, the treatments had opposite effects, with CR increasing and RM decreasing phosphorylation. Thus, RM mitigates aging-associated changes in the phosphorylation mTORC1 substrates, demonstrating that our data accurately capture expected changes. Moreover, as we have previously observed in phenotypic and functional measurements[9], the effects of CR and RM on aging processes only partially overlap in mouse muscles.

We also checked the 9 sites in 6 upstream mTORC1 regulators (Supplementary Data 3) represented in our data. The most consistent changes in phosphorylation across muscles were in the proline-rich AKT1 substrate 1 (Akt1s1/Pras40), an endogenous inhibitor of mTORC1 that binds regulatory-associated protein of mTOR (Rptor)[20,21] (Fig. 2A). Akt1s1 is phosphorylated on different sites (S183/184, S212/213, and S221/S222 in human/mouse numbering) by at least 3 kinases to induce its release from mTORC1, thereby allowing its activation[21]. In our data, RM (but not CR) consistently reduced the Akt1s1 phosphorylation on S213 (Fig. 2B), a site reported to be phosphorylated in vitro by mTORC1 in a RM-dependent manner, while in vivo the RM sensitivity and the responsible kinase are unclear (reviewed in ref. 22). The S202/S203 and 203/204 (human/mouse) in Akt1s1 were reported to undergo phosphorylation by pyruvate kinase PKM-isoform M2 (Pkm2) in cancer[23], leading to Akt1s1 dissociation from Rptor and release of mTORC1 inhibition[23]. Here we found that the S204 signal was increased by AGE in 3 out of 4 muscles (Fig. 2C), while CR and especially RM mitigated S204 phosphorylation (Fig. 2B). These results are consistent with the previously reported mTORC1 hyperactivity in aged animals, counteracted by the treatments[5]. CR and RM also increased Rptor phosphorylation on S722, a well known AMPK site[24], which is expected to inhibit mTORC1 (Fig. 2C).

Finally, we detected 5 phosphosites in 5 of the 30 direct substrates of mTORC2 (Supplementary Data 3). Interestingly, these were all upregulated in AGE (Fig. 2D), indicating that not only mTORC1 but also mTORC2 activity increases in aging muscle. The Akt2 S450 and protein kinase C alpha type (Prkca) T638 sites are known as "turn motif" (TM) sites and are cotranslationally phosphorylated by mTORC2 to stabilize the proteins (reviewed in ref. 6). That CR and RM reduce the phosphorylation of these sites is consistent with previous reports of mTORC2 inhibition upon prolonged RM treatment[25,26]. Altogether, these observed patterns of protein phosphorylation support the notion that not only mTORC1 but also mTORC2 activities increase during aging, and that CR and especially RM mitigate this increase to maintain muscle functionality[9].

General changes induced by AGE, CR, and RM in annotated phosphosites

The analysis of mTOR pathway components showed that we recovered expected changes in protein phosphorylation during aging and upon RM treatment, but also revealed substantial variation in the response of individual muscles to the treatments (Supplementary Fig. 2). Between-muscle differences were more pronounced than those induced by AGE, CR or RM (Fig. 1C). PCA of data from individual muscles showed that for *soleus* and *tibialis anterior* 10M_WT and 30M_WT samples separated along PC1, for *triceps* 10M_WT and 30M_WT samples separate along PC2, while for *gastrocnemius* samples do not clearly separate on any PC (Supplementary Fig. 2). To identify biological processes most generally affected by AGE, CR, and RM, we extracted phosphosites showing common changes in all four muscles. 227, 291, and 172 phosphopeptides were significantly regulated in all muscles in the AGE, CR, and RM conditions, respectively (Supplementary Figs. 3, 4). As previously noted, only a small proportion of these have cognate kinases annotated in the PhosphoSitePlus database[27]. Therefore, we refer to sites as annotated, unannotated or novel, depending on their presence/absence in PhosphoSitePlus and whether a cognate kinase has been reported.

Broadly, AGE-associated changes in the phosphorylation of annotated sites (Fig. 3A, B) occur in many aging-relevant processes, including stress granule formation (Ras GTPase-activating protein-binding protein 1 (G3bp1) S149 phosphorylation[28]), formation of actin stress fibers (cytoskeleton-associated protein 1, Cap-1 S307[29]), autophagy (Sequestosome-1 (Sqstm1) T269[30]), and fatty acid metabolism (acetyl-coA carboxylase, also known as Acc1 or Acaca[31]). The AMPK catalytic subunit alpha-1 (Ampka1), a cellular sensor of energy levels[32] is the kinase associated with most of the AGE-dependent sites. The CR and RM treatments do not consistently mitigate the AGE-associated increase in Ampka1 target site phosphorylation, possibly reflecting the variable activity reported for AMPK in different aging-associated conditions[33,34].

The phosphosites that are generally and significantly altered by CR are associated with diverse kinases and impact cell adhesion, motility, pluripotency, and differentiation (Fig. 3C, D). In particular, the CR-reduced S236 phosphorylation in Rps6 may reflect the suppression of mTORC1 activity by dietary restriction. Finally, the general and significant effects of RM are strongly localized to the mTORC1 pathway (Fig. 3E, F), where RM counteracts aging-associated increases in phosphorylation. In addition, RM increases the phosphorylation of some Camk2b substrates, including Camk2b itself, across all muscles, which is intriguing given that Camk2b plays an important role in synaptic transmission[35], and neuromuscular junctions (NMJs) are remodeled during aging[5].

CR and RM mitigate aging-induced changes in unannotated phosphosites

Next, we asked whether CR or RM also mitigate aging-induced changes in phosphosites without annotated kinases. There were 204, 255, and 150 kinase-unannotated phosphosites that changed consistently in all muscles with AGE, CR, and RM, respectively (Fig. 4A). The 3 phosphosites that underwent significant changes in all muscles and all conditions were located in proteins not known so far to play a role in the context of aging (Fig. 4A). We then turned to phosphosites that showed consistent changes across muscles in at least two conditions, as these could provide novel targets for anti-aging interventions or highlight side-effects of anti-aging treatments. The treatments generally mitigated AGE effects, with signal intensity changes occuring in opposite directions for AGE than CR or RM effects (Fig. 4). Only one site, S1937 in the cytoskeleton-associated ankyrin-3 (Ank3) protein, underwent significant changes in the same direction across all muscles and conditions, with a more pronounced AGE effect than that mediated by RM or CR (Fig. 4B).

Phosphopeptides whose aging-associated change was mitigated by CR across muscles (Fig. 4B, C) come from neurofilaments (heavy (Nefh) and medium (Nefm)), proteins associated with the endoplasmic reticulum and related stress responses (UBX domain-containing protein 6 (Ubxn6), protein disulfide-isomerase A6 (Pdia6), endoplasmic reticulum chaperone BiP (Hspa5), nascent polypeptide-associated complex subunit alpha (Naca)), as well as from proteins involved in vesicular trafficking (target of Myb1 membrane trafficking protein (Tom1) and synaptotagmin-2 (Syt2)).

RM acts on a different set of targets, mitigating aging-induced phosphorylation changes of proteins involved in glucose metabolism (TBC1 domain family member 4 (Tbc1d4)), mitochondria (sarcoplasmic/endoplasmic reticulum calcium ATPase 1 (Atp2a1)), TAR DNA-binding protein 43 (Tardbp) and muscle structure (e.g., dystrophin (Dmd), Fig. 4D). RM also increased the phosphorylation of a C-terminal serine (S1502) in synemin (Synm), a protein essential for cell adhesion and migration[36].

A few phosphosites responded significantly across all muscles to anti-aging interventions, but not to AGE itself. CR and RM increased the phosphorylation signal of sites in the muscle contraction-related proteins filamin C (Flnc), leiomodin 2 (Lmod2), and myosin binding protein H (Mybph) as well as the neurofilament protein Nefm. BCL2/adenovirus E1B 19 kDa protein-interacting protein 3 (Bnip3), a protein that mediates mitophagy under stress[37], also showed increased treatment-induced phosphorylation. The AGE effect on phosphosites was inconsistent across muscles and it

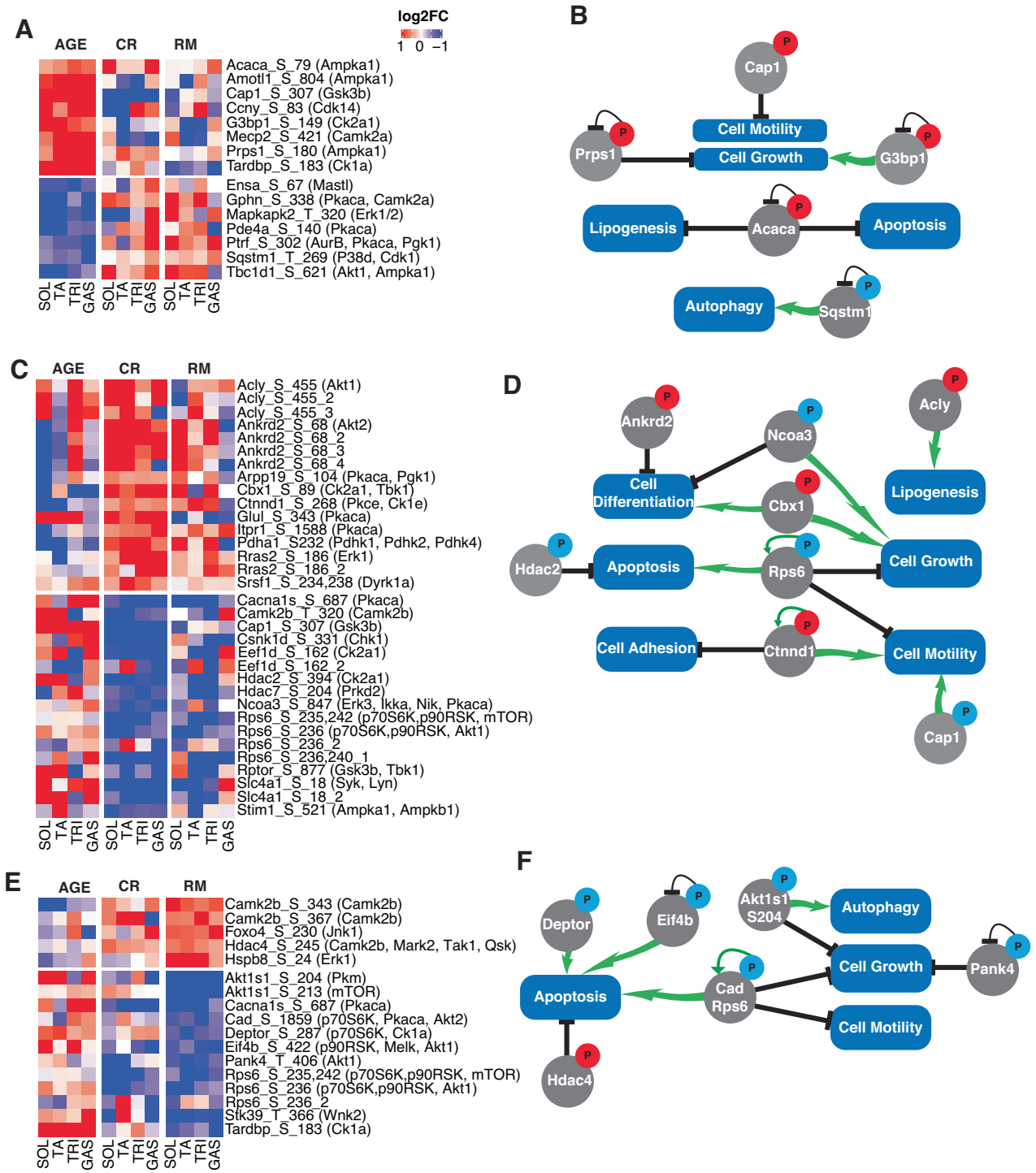

Fig. 3 | General changes induced by individual treatments across all muscles. **A** Kinase and functionally-annotated phosphorylation sites that are significantly altered by AGE in all muscles (log2 fold changes capped at ±1). Relative changes in phosphopeptide intensity are shown for all muscles and all conditions. The site coordinate within the protein is shown, along with the protein kinase known to phosphorylate the site. If a phosphosite was covered by multiple peptides, the individual peptides are shown, indicated by an additional number in the name. **B** Biological processes in which the phosphorylation sites from (**A**) play a role according to the PhosphoSitePlus database. The direction of the phosphorylation signal change is indicated by the red (increase) and blue (decrease) color of the phosphate symbol, and the effect of the phosphorylation on the process is indicated by the color of the arrows leading to the respective process, black for repression and green for activation. If the phosphorylation modifies the activity of the substrate protein, the activity change upon phosphorylation is indicated by the arrow leading to the substrate (black - inhibition, green - activation). **C** Similar to (**B**), for CR-altered sites. **D** Same as in (**C**), for CR-altered phosphopeptides. **E** Similar to (**B**), for RM-altered sites. **F** Same as in (**C**), for RM-altered phosphopeptides.

remains to be determined whether these sites are undesired targets of CR and RM or provide unexpected benefits. A few phosphosites displayed lower phosphorylation in response to CR and RM, while displaying higher, but less consistent, phosphorylation during AGE. These proteins are involved in muscle structure (titin, Ttn), contraction (sarco(endo)plasmic reticulum calcium-ATPase 1 (SERCA1) also known as Atp2a1) and glycogen breakdown (skeletal muscle isoform of Phosphorylase B Kinase Regulatory Subunit Alpha, Phka1).

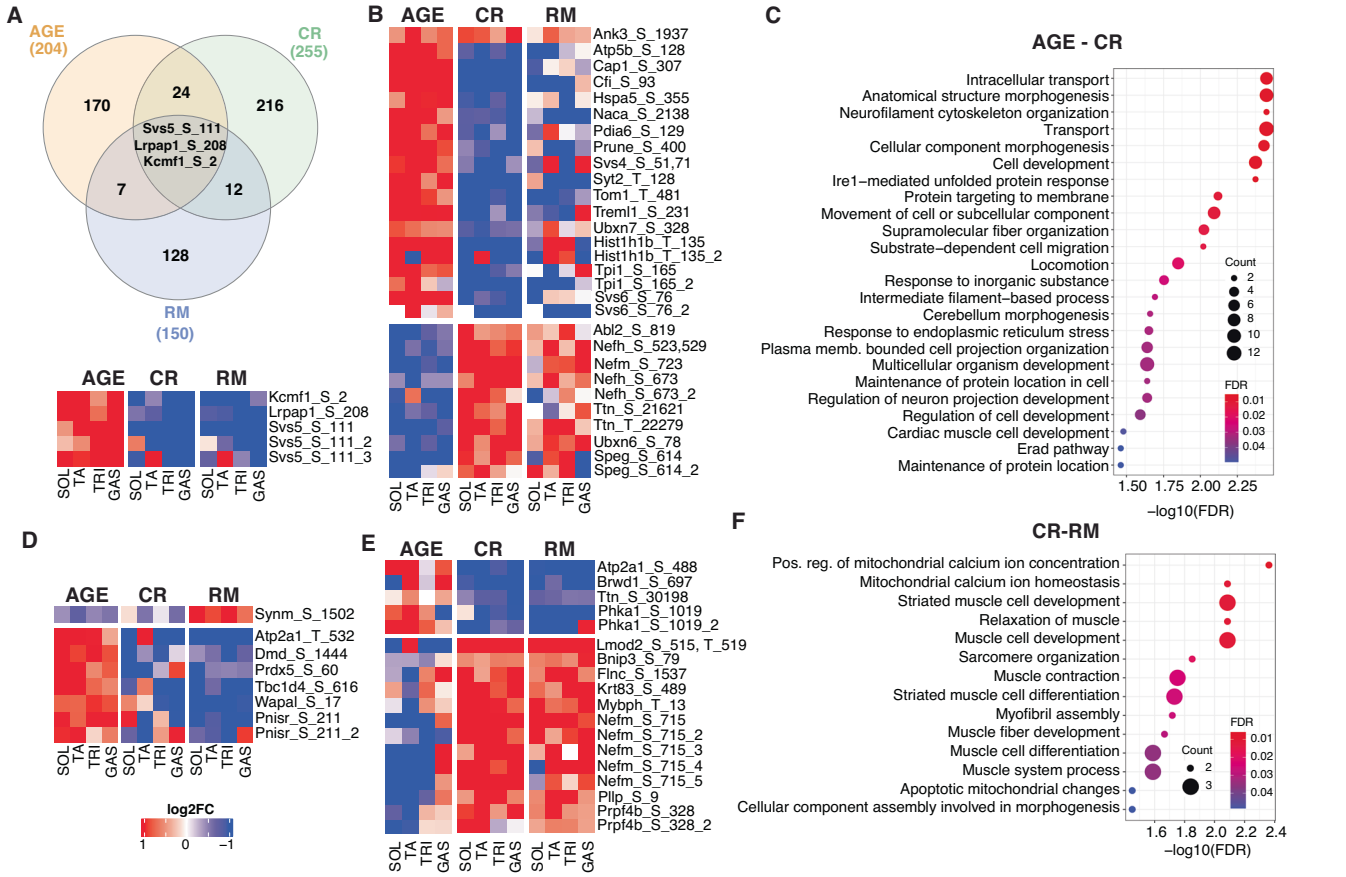

Fig. 4 | Conserved but unannotated protein phosphorylation sites in muscles of aged, treated and untreated mice. A Top: Venn diagram showing the overlap between phosphosites that responded consistently across all four muscles in AGE, CR, and RM treatments. Shown are sites without an annotated kinase. Bottom: log2 fold changes in the intensity of the indicated peptides in each condition and each of the four muscles. Shown are the phosphopeptides that changed significantly and consistently in all muscles in all three conditions. Same as in (**A**) but conditioned on significant and consistent changes across muscles in AGE and CR (**B**), AGE and RM (**D**) and CR and RM (**E**). **C** Significantly enriched biological processes (GO terms) in proteins with consistently changing phosphosite in AGE and CR. **F** Same as (**C**) but for proteins with consistently changing phosphosite in CR and RM.

Therefore, our data show that CR and RM mitigate the AGE-induced reduction in phosphorylation signal of proteins involved in cell adhesion, muscle contraction, and neuronal function. The two treatments exert largely consistent, but quantitatively distinct effects. Furthermore, for many sites that undergo significant changes in all muscles a cognate kinase has not been reported. Identifying the cognate kinases would further enhance our understanding of skeletal muscle aging.

Kinase activity signatures of individual muscles

While the coverage of phosphosites in any given experiment is still incomplete, changes in individual kinase activity between conditions can be robustly inferred by kinase set enrichment analysis (KSEA)[38], based on coherent signal intensity changes in the multiple substrates targeted by a specific kinase (Fig. 5A). Age-related kinase activity patterns varied widely across the four muscles (Fig. 5B), while CR and RM again generally counteracted these changes. The most salient changes were the AGE-associated reduction in Akt2 activity and the increase in Mapk14/p38α activity in both *soleus* and *tibialis anterior* muscles, each of which was counteracted by CR and RM. In *gastrocnemius* muscle, CR, but not RM, also counteracted the effects of AGE on Akt2 and Mapk14/p38α activity.

As kinase activity is typically regulated by phosphorylation, we also examined the complex dynamics of phosphorylation sites located on the kinases themselves (Fig. 5C–E). Among the more consistent changes were the RM-mediated suppression of the age-related increase in stress response-linked protein Ste20/Sps1-related proline-alanine-rich protein kinase (Stk39)[39] phosphorylation, the CR-mediated increase in 6-phosphofructo-2-kinase/fructose-2,6-bisphosphatase 2 (Pfkfb2)[40] and Glycogen synthase kinase-3 alpha (Gsk3a) phosphorylation, as well as the RM-mediated increase in multiple phosphosites on Camk2b, a kinase with important roles in neuronal plasticity[41] and NMJ stability[42]. RM upregulated the autophosphorylation of Camk2b T287, which makes Camk2b persistently active even when calcium concentrations are low[43]. Autophosphorylated Camk2b has been shown to phosphorylate histone deacetylase 4 (Hdac4) on S245 to promote its nuclear export[44]. Indeed, RM also increased Hdac4 S245 phosphorylation across all 4 muscles (Fig. 3E, F). As Hdac4 participates in the muscles response to denervation[45], it would be interesting to further investigate a potential role for Camk2b at the NMJ during aging.

This analysis reveals that RM and CR counteract age-related changes in kinase activities, but that the effects of individual kinases are quantitatively different between muscles, making it challenging to generalize data obtained in a specific system.

Expanding the atlas of protein phosphorylation sites

In this study we detected 6960 non-redundant phosphosites in at least 2 samples, with 6526 detected in at least 48 of the 95 samples. 5545 of the 6960 sites are already represented in the PhosphoSitePlus database and 485 also have an annotated kinase. However, 1415 are not represented in this database, i.e., they are novel. The known phosphorylation sites come from 597 proteins and the novel sites from 227 proteins, with 208 proteins in the overlap (Fig. 6A). Thus, we have identified 19 novel phosphoproteins in the mouse (Fig. 6A). Both annotated and novel sites are located in proteins involved in muscle development, muscle cell organization, and contraction,

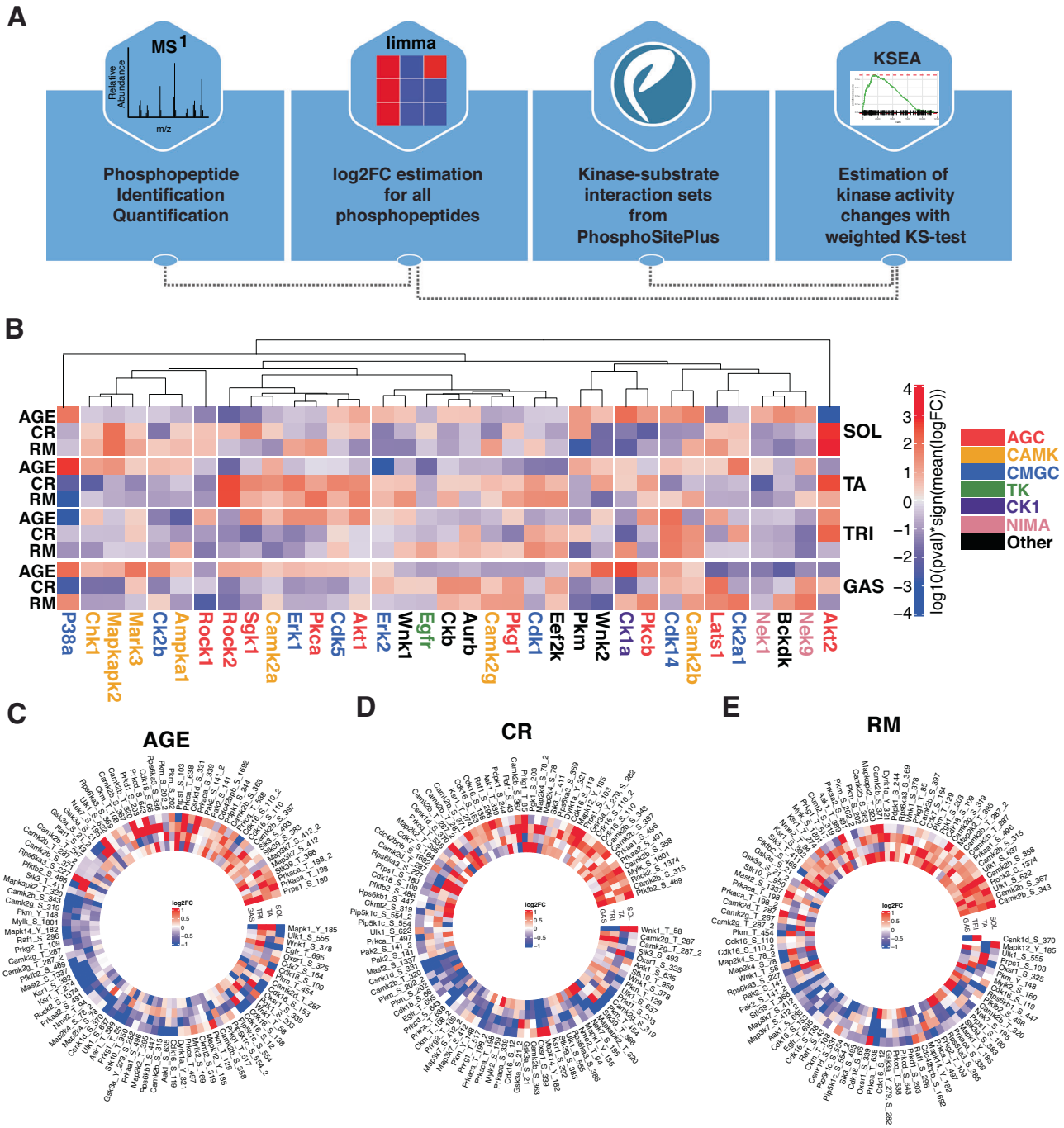

Fig. 5 | Muscle-specific kinase signatures. A Illustration of KSEA[38]. **B** Kinases with significant changes in activity between conditions. Each line corresponds to a kinase that has a significant activity change ($p < 0.05$) in at least one muscle and one condition. The color indicates the class of the kinase. **C**–**E** Changes in kinase phosphorylation level in AGE, CR, and RM, respectively. Each ring shows the change in phosphosite (indicated by the label) intensity in the respective condition in one muscle.

as well as energy metabolism (Fig. 6B, Supplementary Data 1). Importantly, absolute intensity of known and novel phosphoproteins were comparable (Fig. 6C), indicating that low protein expression levels cannot account for these novel sites having been overlooked. Furthermore, we did not observe any muscle- or condition-specific expression of the novel phosphosites or phosphorylated proteins (Fig. 6D). However, data from the Human Protein Atlas[46] indicate that the expression of genes corresponding to these novel phosphosites is largely restricted to muscle tissue (Fig. 6E–H), which may be underrepresented in proteomics datasets compared to other tissues (e.g., liver or lung). This suggests a more specific context of functionality for the novel sites and underscores the importance of broad surveys that cover multiple organs and multiple interventions.

Our data substantially expand the muscle phosphoproteome and enhance the information about the conditions and specific muscles in which these sites are modified.

Discussion

Aging processes have raised substantial interest in recent years, enabled by the numerous technologies for comprehensive gene expression profiling. Bulk RNA-seq, single cell RNA-seq, and single nucleus RNA-seq have been

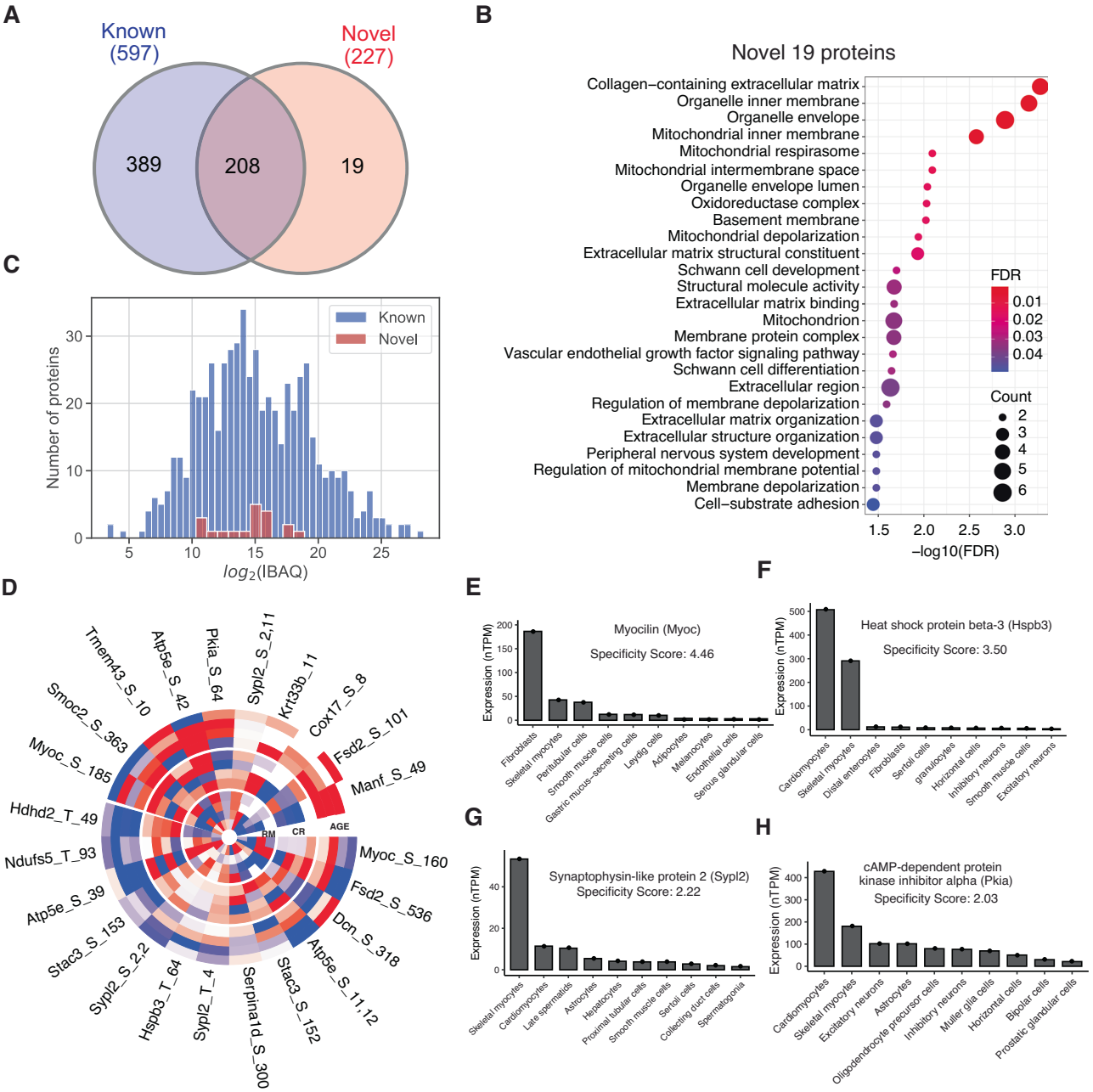

Fig. 6 | Expanding the atlas of protein phosphorylation sites. A Venn diagram showing the relationship of proteins with already annotated vs. novel sites. **B** Gene Ontology overrepresentation analysis of novel *Mus musculus* phosphoproteins. **C** Histogram of protein abundances for proteins containing annotated phosphosites (blue) vs. those containing novel sites (red). **D** Log2 fold change in phosphopeptide signal intensity in the AGE, CR, and RM conditions for phosphosites located in the 19 novel phosphoproteins that are common to all 4 muscles. The order of the muscles in the circular representation from outside to inside is *soleus*, *tibialis anterior*, *triceps,* and *gastrocnemius*. **E**–**H** Single cell RNA-seq data from Human Protein Atlas[46] showing the distribution of RNA expression levels for 4 of the novel mouse phosphoproteins (tissue specificity score based on[75]). Data are represented as dots overlayed over corresponding bars.

used to determine the cell type composition and gene expression in the tissues of young and aged mice as well as humans[47–49]. A transcriptomic atlas of skeletal muscle aging has thus been derived, revealing cellular senescence as a conserved mechanism of skeletal muscle aging, which may contribute to sarcopenia[50,51]. While aging is intrinsic to life, a variety of interventions have been shown to counteract aging-associated changes and extend healthspan[52]. In particular, consistent with deregulated nutrient signaling being one of the twelve currently recognized hallmarks of aging[53], CR and RM, a drug that inhibits the activity of the mTORC1 complex involved in nutrient sensing, increase the lifespan and/or healthspan of animals[54,55]. The effects of long-term suppression of nutrient signaling pathways by CR and RM still remain to be unraveled, though it has already been shown that different muscles have distinct functional responses to these interventions[9]. Specifically, CR was found to improve body-mass-normalized *soleus* mass, while RM to more effectively prevent the age-related decline in *triceps* mass[9]. The mechanistic basis of these different functional responses is yet unclear, as very few studies have attempted to determine the signaling dynamics underlying gene expression changes during aging and following anti-aging interventions. Our study comes to fill this gap, making the following contributions.

First, we provide the most extensive protein phosphorylation data set during aging and following long-term CR and RM treatments. While the effects of short and long-term anti-aging treatments on various mouse organs have been studied before, our data set covers four distinct muscles

that were analyzed before at the mRNA level, providing comprehensive complementary data on signaling via protein phosphorylation and highlighting between-muscle differences in signaling that likely underlie the differences in their functional response to AGE, CR, and RM. Overall, we reproducibly identified 6960 phosphosites, 1415 of which are not represented in the main repository of the field, the PhosphoSitePlus database[56]. While newly-identified sites are generally located in known phosphoproteins, 26 phosphosites were located in 19 proteins not previously known to contain phosphorylation sites in mice. These proteins are associated with neurofilaments, mitochondria, and muscle contraction and their expression is specific to muscle (Fig. 6). Due to the transient nature of signaling and limited life times of phosphorylation states it can be difficult to capture them experimentally when their expression is restricted to particular tissues.

Second, we surveyed the dynamics of protein phosphorylation in the mTOR pathway following long-term interventions impinging on this pathway. Our results confirm the inhibitory effect of RM not only on mTORC1 but also on some mTORC2 substrates (Fig. 2). Interestingly, the substrates of Rps6kb, a key rapamycin sensitive readout of mTORC1 activity, exhibited a more consistent reduction in phosphorylation than the substrates of mTORC1 itself. This could reflect differences in the sensitivity of mTORC1-substrate interactions to RM[57] or feedback regulation during the very long-term treatment with RM, which would be interesting to explore in further work. While CR shared some aspects of RM's effect on the mTOR pathway, RM exerted more uniform changes across muscles than CR (Fig. 2). In line with previously described differences in muscle properties[9], this observation reinforces the notion that RM exerts a more targeted suppression of mTORC1 signaling than CR.

Third, we identified numerous sites where CR and RM exert phosphorylation changes antagonistic to those mediated by AGE (Figs. 3, 4). Interestingly, aging was accompanied by increased phosphorylation signals in diverse proteins and counteracted by CR and RM. In contrast, phosphorylation signals in structural components of the muscle (neurofilament proteins Nefm and Nefh, Mybph, Lmod2, Flnc) decreased at high age, but were increased by the treatments. While studies of protein phosphorylation following anti-aging interventions are scarce, CR was recently reported to restore a "youthful" protein phosphorylation landscape in mouse *quadriceps* muscle, primarily via Pka[58]. Our broader study, based on a different CR regimen and involving multiple muscle types lends further support to those results, indicating that different kinases may drive the changes observed in different muscles. In particular, KSEA suggests prominent roles for Akt2 and Mapk14/p38α, whose aging-associated changes are mitigated by both treatments in *soleus* and *tibialis anterior* muscles, and by CR in *gastrocnemius* (Fig. 5B). Prior work in the worm *Caenorhabditis elegans* showed that phosphorylation sites on Akt1 and EIF2α promote longevity, while sites in CK2[59] and Cdk1 limit longevity. Akt2 is the predominant isoform in mouse skeletal muscle and is required for muscle differentiation[60]. Furthermore, Akt1/2 double knockout mice exhibit premature sarcopenia and insulin resistance[61]. In addition to the consistent changes in Akt2 and Mapk14/p38α activity across multiple muscles, many age-related changes in kinase activity were mitigated by both treatments in muscle-restricted manners. For example, the age-related reduction in Rock2 activity was robustly restored by CR and RM in *tibialis anterior*, but not *triceps* or *gastrocnemius*. Rock2 is an exercise-responsive kinase that improves insulin sensitivity in obese animals[62]. Another kinase with muscle-specific activity patterns was Camk2b, a potential downstream target of Mapk14/p38α in denervation-induced atrophy[63]. This could be interesting to study further, in the context of muscle-specific responses to age-related denervation[5]. To facilitate the interpretation of kinase activity changes, we also summarized the behavior of regulatory phosphorylation sites located within kinases (Fig. 5C).

To conclude, our study provides a broad view of phosphorylation-dependent changes in signaling pathways that occurred in four distinct mouse muscles during aging, and in response to long-term anti-aging interventions, specifically CR and RM. These serve as a basis for an improved understanding of aging processes and for novel treatment targets aiming to improve muscle functionality in aging individuals.

Methods

Muscle samples

Snap frozen muscles of male C57BL/6JRj mice were obtained from our previous studies[5,9]. In the week immediately prior to starting the experiment, body mass, food intake, grip strength, and body composition (via EchoMRI) were measured and used for balanced group selection. 10-month-old mice were used as an adult control (10M_WT), while 15-month-old mice received either a control AIN-93M diet containing Eudragit (vehicle) *ad libitum* (30M_WT), a calorie restricted diet (30M_CR; 65% of standard diet without restricting vitamins and minerals) or a diet containing 42 mg/kg chow active encapsulated (Eudragit) RM (30M_RM) from the age of 15 to 30 months. Based on measured food intake, mice received a RM dose of 4.2 mg/kg body mass/day. Due to the calorie restriction group, all mice were single caged. Prior to tissue collection, food was removed from the cages in the early morning. Mice were sacrificed within the same 3–4 h period from late morning. All procedures were performed in accordance with Swiss regulations for animal experimentation and approved by the veterinary commission of the Canton Basel-Stadt. We have complied with all relevant ethical regulations for animal use.

Phospho - and proteome LC-MS analysis

Around 3 mg of muscle tissue was excised, snap frozen, and mechanically grinded followed by lysis in 8 M Urea (Sigma), 0.1 M ammonium bicarbonate in presence of phosphatase inhibitors (Sigma P5726&P0044) using strong ultra-sonication (Bioruptor, 10 cycles, 30 s on/off, Diagenode, Belgium). Protein concentration was determined by BCA assay (Thermo Fisher Scientific) using a small sample aliquot. 200 µg of proteins were digested as described previously[64], reduced with 5 mM TCEP for 60 min at 37 °C and alkylated with 10 mM chloroacetamide for 30 min at 37 °C. After diluting samples with 100 mM ammonium bicarbonate buffer to a final urea concentration of 1.6 M, proteins were digested by incubation with sequencing-grade modified trypsin (1/50, w/w; Promega, Madison, Wisconsin) overnight at 37 °C. After acidification using 5% TFA, peptides were desalted on C18 reversed-phase spin columns according to the manufacturer's instructions (Macrospin, Harvard Apparatus) and dried under vacuum.

Peptide samples were enriched for phosphorylated peptides using Fe(III)-IMAC cartridges on an AssayMAP Bravo platform as described[65]. The setup of the µRPLC-MS system was as described previously[64]. Chromatographic separation of peptides was carried out using an EASY nano-LC 1000 system (Thermo Fisher Scientific), equipped with a heated RP-HPLC column (75 µm × 37 cm) packed in-house with 1.9 µm C18 resin (Reprosil-AQ Pur, Dr. Maisch). Aliquots of 1 µg total phosphopeptides were analyzed per LC-MS/MS run using a linear gradient ranging from 95% solvent A (0.15% formic acid, 2% acetonitrile) and 5% solvent B (98% acetonitrile, 2% water, 0.15% formic acid) to 30% solvent B over 90 min at a flow rate of 200 nl/min. Mass spectrometry analysis was performed on Q-Exactive HF mass spectrometer equipped with a nanoelectrospray ion source (both Thermo Fisher Scientific). Each MS1 scan was followed by high-collision-dissociation (HCD) of the 10 most abundant precursor ions with dynamic exclusion for 20 s. Total cycle time was approximately 1 s. For MS1, 3e6 ions were accumulated in the Orbitrap cell over a maximum time of 100 ms and scanned at a resolution of 120,000 FWHM (at 200 m/z). MS2 scans were acquired at a target setting of 1e5 ions, accumulation time of 100 ms and a resolution of 30,000 FWHM (at 200 m/z). Singly charged ions and ions with unassigned charge state were excluded from triggering MS2 events. The normalized collision energy was set to 27%, the mass isolation window was set to 1.4 m/z and one microscan was acquired for each spectrum.

In addition, a global proteomics LC-MS analysis was carried out. Here, 0.25 µg of peptides were taken from each sample after phosphopeptide enrichment and subjected to LC–MS/MS analysis using a Orbitrap Fusion

Lumos Mass Spectrometer fitted with an EASY-nLC 1200 (both Thermo Fisher Scientific) and a custom-made column heater set to 60 °C. Peptides were resolved using a RP-HPLC column (75 µm × 36 cm) packed in-house with C18 resin (ReproSil-Pur C18–AQ, 1.9 µm resin; Dr. Maisch GmbH) at a flow rate of 0.2 µLmin-1. The following gradient was used for peptide separation: from 5% B to 12% B over 5 min to 35% B over 65 min to 50% B over 20 min to 95% B over 2 min followed by 18 min at 95% B. Buffer A was 0.1% formic acid in water and buffer B was 80% acetonitrile, 0.1% formic acid in water. The mass spectrometer was operated in DDA mode with a cycle time of 3 s between master scans. Each master scan was acquired in the Orbitrap at a resolution of 120,000 FWHM (at 200 m/z) and a scan range from 375 to 1500 m/z followed by MS2 scans of the most intense precursors in the linear ion trap at "Rapid" scan rate with isolation width of the quadrupole set to 1.4 m/z. Maximum ion injection time was set to 50 ms (MS1) and 35 ms (MS2) with an AGC target set to 1e6 and 1e4, respectively. Only peptides with charge state 2–5 were included in the analysis. Monoisotopic precursor selection (MIPS) was set to Peptide, and the Intensity Threshold was set to 5e3. Peptides were fragmented by HCD (Higher-energy collisional dissociation) with collision energy set to 35%, and one microscan was acquired for each spectrum. The dynamic exclusion duration was set to 30 s.

Analysis of LC-MS data

The acquired raw-files were imported into the Progenesis QI software (v2.0, Nonlinear Dynamics Limited), which was used to extract peptide precursor ion intensities across all samples applying the default parameters. The generated mgf-files were searched using MASCOT against a decoy database containing normal and reverse sequences of the predicted SwissProt entries of *Mus musculus* (www.ebi.ac.uk, release date 2016/11/15) and commonly observed contaminants (in total 33,984 sequences) generated using the SequenceReverser tool from the MaxQuant software (Version 1.0.13.13). The search criteria were set as follows: full tryptic specificity was required (cleavage after lysine or arginine residues, unless followed by proline); 3 missed cleavages were allowed; carbamidomethylation (C) was set as fixed modification; oxidation (M) and phosphorylation (STY) (only for phosphopeptide enriched data) were applied as variable modifications; mass tolerance of 10 ppm (precursor) and 0.02/0.6 Da (fragments) for phoshoproteomics/proteomics data analysis. The database search results were filtered using the ion score to set the false discovery rate to 1% on the peptide and protein level, respectively, based on the number of reverse protein sequence hits in the datasets. The relative quantitative data obtained were normalized and statistically analyzed using *limma* R package[66] version 3.64.0. The custom scripts for analyzing the phosphoproteomics data are deposited on Zenodo with DOI: 10.5281/zenodo.10635552.

Gene Ontology (GO) overrepresentation analysis

The ClusterProfiler[67] R package version 3.18.1 was used for all the GO term analyses reported in this study. ComplexHeatmap[67,68] version 2.6.2 and circlize[69] version 0.4.15 R packages were used to construct the heatmaps. InteractiVenn[70] was used for Venn diagrams.

Identification of phosphopeptides changes independent of expression levels

We applied a two-tailed t-test to compare the normalized protein intensities from a muscle of interest (e.g., *soleus*) and the rest of the samples (e.g., all samples from *tibialis anterior*, *triceps,* and *gastrocnemius*) for the genes with phosphopeptides that correlate with the principal component (PC) of interest. If the *p* value from the t-test is bigger than the threshold (0.05), it indicates that the changes in phosphopeptide level cannot be explained by changes in the protein level. If *p* value is smaller than the threshold, and the direction of the change in protein expression and phosphopeptide level is opposite, then the phosphopeptide changes cannot be attributed to changes in protein levels.

Reporting summary

Further information on research design is available in the Nature Portfolio Reporting Summary linked to this article.

Data availability

All mass spectrometry proteomics data associated with this manuscript is available from the ProteomicsXchange consortium via MassIVE (https://massive.ucsd.edu), with the accession number MSV000093798. Data needed to evaluate the conclusions of the paper are present in the paper and/or the Supplementary Materials.

Received: 24 March 2024; Accepted: 2 August 2024;
Published online: 10 August 2024

References

1. Niccoli, T. & Partridge, L. Ageing as a risk factor for disease. *Curr. Biol.* **22**, R741–R752 (2012).
2. Siparsky, P. N., Kirkendall, D. T. & Garrett, W. E. Jr. Muscle changes in aging: understanding sarcopenia. *Sports Health* **6**, 36–40 (2014).
3. Evans, W. J. Skeletal muscle loss: cachexia, sarcopenia, and inactivity. *Am. J. Clin. Nutr.* **91**, 1123S–1127S (2010).
4. Sandri, M. et al. Signalling pathways regulating muscle mass in ageing skeletal muscle: the role of the IGF1-Akt-mTOR-FoxO pathway. *Biogerontology* **14**, 303–323 (2013).
5. Ham, D. J. et al. The neuromuscular junction is a focal point of mTORC1 signaling in sarcopenia. *Nat. Commun.* **11**, 4510 (2020).
6. Battaglioni, S., Benjamin, D., Wälchli, M., Maier, T. & Hall, M. N. mTOR substrate phosphorylation in growth control. *Cell* **185**, 1814–1836 (2022).
7. Castets, P. et al. Sustained activation of mTORC1 in skeletal muscle inhibits constitutive and starvation-induced autophagy and causes a severe, late-onset myopathy. *Cell Metab.* **17**, 731–744 (2013).
8. Stallone, G., Infante, B., Prisciandaro, C. & Grandaliano, G. mTOR and aging: old fashioned dress.*Int. J. Mol. Sci.* **20**, 2774 (2019).
9. Ham, D. J. et al. Distinct and additive effects of calorie restriction and rapamycin in aging skeletal muscle. *Nat. Commun.* **13**, 2025 (2022).
10. Cesaro, L. & Pinna, L. A. Prevalence and significance of the commonest phosphorylated motifs in the human proteome: a global analysis. *Cell. Mol. Life Sci.* **77**, 5281–5298 (2020).
11. Hornbeck, P. V. et al. PhosphoSitePlus, 2014: mutations, PTMs and recalibrations. *Nucleic Acids Res.* **43**, D512–D520 (2015).
12. Huckstep, H., Fearnley, L. G. & Davis, M. J. Measuring pathway database coverage of the phosphoproteome. *PeerJ* **9**, e11298 (2021).
13. Savage, S. R. & Zhang, B. Using phosphoproteomics data to understand cellular signaling: a comprehensive guide to bioinformatics resources. *Clin. Proteom.* **17**, 27 (2020).
14. Umek, N., Horvat, S. & Cvetko, E. Skeletal muscle and fiber type-specific intramyocellular lipid accumulation in obese mice. *Bosn. J. Basic Med. Sci.* **21**, 730–738 (2021).
15. Lamming, D. W. Inhibition of the Mechanistic Target of Rapamycin (mTOR)-Rapamycin and beyond. *Cold Spring Harb. Perspect. Med.* **6**, a025924 (2016).
16. Kapadia, B. B., Roychowdhury, A., Kayastha, F., Nanaji, N. & Gartenhaus, R. B. PARK2 regulates eIF4B-driven lymphomagenesis. *Mol. Cancer Res.* **20**, 735–748 (2022).
17. Kaeser-Pebernard, S. et al. mTORC1 controls Golgi architecture and vesicle secretion by phosphorylation of SCYL1. *Nat. Commun.* **13**, 4685 (2022).
18. Zi, Z. et al. Quantitative phosphoproteomic analyses identify STK11IP as a lysosome-specific substrate of mTORC1 that regulates lysosomal acidification. *Nat. Commun.* **13**, 1760 (2022).
19. Barilari, M. et al. ZRF1 is a novel S6 kinase substrate that drives the senescence programme. *EMBO J.* **36**, 736–750 (2017).

20. Oshiro, N. et al. The proline-rich Akt substrate of 40 kDa (PRAS40) is a physiological substrate of mammalian target of rapamycin complex 1. *J. Biol. Chem.* **282**, 20329–20339 (2007).
21. Wang, L., Harris, T. E. & Lawrence, J. C. Jr. Regulation of proline-rich Akt substrate of 40 kDa (PRAS40) function by mammalian target of rapamycin complex 1 (mTORC1)-mediated phosphorylation. *J. Biol. Chem.* **283**, 15619–15627 (2008).
22. Wiza, C., Nascimento, E. B. M. & Ouwens, D. M. Role of PRAS40 in Akt and mTOR signaling in health and disease. *Am. J. Physiol. Endocrinol. Metab.* **302**, E1453–E1460 (2012).
23. He, C.-L. et al. Pyruvate kinase M2 activates mTORC1 by phosphorylating AKT1S1. *Sci. Rep.* **6**, 21524 (2016).
24. Gwinn, D. M. et al. AMPK phosphorylation of raptor mediates a metabolic checkpoint. *Mol. Cell* **30**, 214–226 (2008).
25. Lamming, D. W. et al. Rapamycin-induced insulin resistance is mediated by mTORC2 loss and uncoupled from longevity. *Science* **335**, 1638–1643 (2012).
26. Mannick, J. B. & Lamming, D. W. Targeting the biology of aging with mTOR inhibitors. *Nat. Aging* **3**, 642–660 (2023).
27. Ghosh, S. et al. CFIm-mediated alternative polyadenylation remodels cellular signaling and miRNA biogenesis. *Nucleic Acids Res.* **50**, 3096–3114 (2022).
28. Yang, P. et al. G3BP1 is a tunable switch that triggers phase separation to assemble stress granules. *Cell* **181**, 325–345.e28 (2020).
29. Zhou, G.-L., Zhang, H., Wu, H., Ghai, P. & Field, J. Phosphorylation of the cytoskeletal protein CAP1 controls its association with cofilin and actin. *J. Cell Sci.* **127**, 5052–5065 (2014).
30. Zhang, C. et al. Autophagic sequestration of SQSTM1 disrupts the aggresome formation of ubiquitinated proteins during proteasome inhibition. *Cell Death Dis.* **13**, 615 (2022).
31. Monteuuis, G., Suomi, F., Kerätär, J. M., Masud, A. J. & Kastaniotis, A. J. A conserved mammalian mitochondrial isoform of acetyl-CoA carboxylase ACC1 provides the malonyl-CoA essential for mitochondrial biogenesis in tandem with ACSF3. *Biochem. J.* **474**, 3783–3797 (2017).
32. Garcia, D. & Shaw, R. J. AMPK: mechanisms of cellular energy sensing and restoration of metabolic balance. *Mol. Cell* **66**, 789–800 (2017).
33. Hardie, D. G., Ross, F. A. & Hawley, S. A. AMPK: a nutrient and energy sensor that maintains energy homeostasis. *Nat. Rev. Mol. Cell Biol.* **13**, 251–262 (2012).
34. Burkewitz, K., Zhang, Y. & Mair, W. B. AMPK at the nexus of energetics and aging. *Cell Metab.* **20**, 10–25 (2014).
35. Thiagarajan, T. C., Piedras-Renteria, E. S. & Tsien, R. W. alpha- and betaCaMKII. Inverse regulation by neuronal activity and opposing effects on synaptic strength. *Neuron* **36**, 1103–1114 (2002).
36. Sun, N., Huiatt, T. W., Paulin, D., Li, Z. & Robson, R. M. Synemin interacts with the LIM domain protein zyxin and is essential for cell adhesion and migration. *Exp. Cell Res.* **316**, 491–505 (2010).
37. He, Y.-L. et al. BNIP3 phosphorylation by JNK1/2 promotes mitophagy via enhancing its stability under hypoxia. *Cell Death Dis.* **13**, 1–13 (2022).
38. Hernandez-Armenta, C., Ochoa, D., Gonçalves, E., Saez-Rodriguez, J. & Beltrao, P. Benchmarking substrate-based kinase activity inference using phosphoproteomic data. *Bioinformatics* **33**, 1845–1851 (2017).
39. Piechotta, K., Garbarini, N., England, R. & Delpire, E. Characterization of the interaction of the stress kinase SPAK with the Na+-K+-2Cl– cotransporter in the nervous system: evidence for a scaffolding role of the kinase. *J. Biol. Chem.* **278**, 52848–52856 (2003).
40. van Gerwen, J. et al. The genetic and dietary landscape of the muscle insulin signalling network. *eLife* **12**, RP89212 (2024).
41. Nicole, O. & Pacary, E. CaMKIIβ in neuronal development and plasticity: an emerging candidate in brain diseases. *Int. J. Mol. Sci.* **21**, 7272 (2020).
42. Martinez-Pena y Valenzuela, I., Mouslim, C. & Akaaboune, M. Calcium/calmodulin kinase II-dependent acetylcholine receptor cycling at the mammalian neuromuscular junction in vivo. *J. Neurosci.* **30**, 12455–12465 (2010).
43. Lisman, J., Yasuda, R. & Raghavachari, S. Mechanisms of CaMKII action in long-term potentiation. *Nat. Rev. Neurosci.* **13**, 169–182 (2012).
44. Backs, J., Song, K., Bezprozvannaya, S., Chang, S. & Olson, E. N. CaM kinase II selectively signals to histone deacetylase 4 during cardiomyocyte hypertrophy. *J. Clin. Investig.* **116**, 1853–1864 (2006).
45. Castets, P. et al. mTORC1 and PKB/Akt control the muscle response to denervation by regulating autophagy and HDAC4. *Nat. Commun.* **10**, 3187 (2019).
46. Karlsson, M. et al. A single-cell type transcriptomics map of human tissues. *Sci. Adv.* **7**, eabh2169 (2021).
47. Kedlian, V. R. et al. Human skeletal muscle aging atlas. *Nat. Aging* **4**, 727–744 (2024).
48. Lai, Y. et al. Multimodal cell atlas of the ageing human skeletal muscle. *Nature* **629**, 154–164 (2024).
49. Tumasian, R. A. 3rd et al. Skeletal muscle transcriptome in healthy aging. *Nat. Commun.* **12**, 2014 (2021).
50. Moiseeva, V. et al. Senescence atlas reveals an aged-like inflamed niche that blunts muscle regeneration. *Nature* **613**, 169–178 (2023).
51. Zhang, X. et al. Characterization of cellular senescence in aging skeletal muscle. *Nat. Aging* **2**, 601–615 (2022).
52. de Cabo, R., Carmona-Gutierrez, D., Bernier, M., Hall, M. N. & Madeo, F. The search for antiaging interventions: from elixirs to fasting regimens. *Cell* **157**, 1515–1526 (2014).
53. López-Otín, C., Blasco, M. A., Partridge, L., Serrano, M. & Kroemer, G. Hallmarks of aging: an expanding universe. *Cell* **186**, 243–278 (2023).
54. Roth, G. S. & Ingram, D. K. Manipulation of health span and function by dietary caloric restriction mimetics. *Ann. N. Y. Acad. Sci.* **1363**, 5–10 (2016).
55. Lee, M. B., Hill, C. M., Bitto, A. & Kaeberlein, M. Antiaging diets: separating fact from fiction. *Science* **374**, eabe7365 (2021).
56. Hornbeck, P. V. et al. 15 years of PhosphoSitePlus®: integrating post-translationally modified sites, disease variants and isoforms. *Nucleic Acids Res.* **47**, D433–D441 (2019).
57. Kang, S. A. et al. mTORC1 phosphorylation sites encode their sensitivity to starvation and rapamycin. *Science* **341**, 1236566 (2013).
58. Bareja, A. et al. Chronic caloric restriction maintains a youthful phosphoproteome in aged skeletal muscle. *Mech. Ageing Dev.* **195**, 111443 (2021).
59. Li, W.-J. et al. Insulin signaling regulates longevity through protein phosphorylation in Caenorhabditis elegans. *Nat. Commun.* **12**, 4568 (2021).
60. Héron-Milhavet, L. et al. Only Akt1 is required for proliferation, while Akt2 promotes cell cycle exit through p21 binding. *Mol. Cell. Biol.* **26**, 8267–8280 (2006).
61. Sasako, T. et al. Deletion of skeletal muscle Akt1/2 causes osteosarcopenia and reduces lifespan in mice. *Nat. Commun.* **13**, 5655 (2022).
62. Muñoz, V. R. et al. Exercise counterbalances Rho/ROCK2 signaling impairment in the skeletal muscle and ameliorates insulin sensitivity in obese mice. *Front. Immunol.* **12**, 702025 (2021).
63. Yuasa, K. et al. Targeted ablation of p38α MAPK suppresses denervation-induced muscle atrophy. *Sci. Rep.* **8**, 9037 (2018).
64. Ahrné, E. et al. Evaluation and improvement of quantification accuracy in isobaric mass tag-based protein quantification experiments. *J. Proteome Res.* **15**, 2537–2547 (2016).
65. Post, H. et al. Robust, sensitive, and automated phosphopeptide enrichment optimized for low sample amounts applied to primary hippocampal neurons. *J. Proteome Res.* **16**, 728–737 (2017).
66. Ritchie, M. E. et al. limma powers differential expression analyses for RNA-sequencing and microarray studies. *Nucleic Acids Res.* **43**, e47 (2015).

67. Yu, G., Wang, L.-G., Han, Y. & He, Q.-Y. clusterProfiler: an R Package for comparing biological themes among gene clusters.*OMICS: J. Integr. Biol.* **16**, 284–287 (2012).
68. Gu, Z., Eils, R. & Schlesner, M. Complex heatmaps reveal patterns and correlations in multidimensional genomic data. *Bioinformatics* **32**, 2847–2849 (2016).
69. Gu, Z., Gu, L., Eils, R., Schlesner, M. & Brors, B. circlize implements and enhances circular visualization in R. *Bioinformatics* **30**, 2811–2812 (2014).
70. Heberle, H., Meirelles, G. V., da Silva, F. R., Telles, G. P. & Minghim, R. InteractiVenn: a web-based tool for the analysis of sets through Venn diagrams. *BMC Bioinform.* **16**, 169 (2015).
71. Peterson, T. R. et al. DEPTOR is an mTOR inhibitor frequently overexpressed in multiple myeloma cells and required for their survival. *Cell* **137**, 873–886 (2009).
72. Duan, S. et al. mTOR generates an auto-amplification loop by triggering the βTrCP- and CK1α-dependent degradation of DEPTOR. *Mol. Cell* **44**, 317–324 (2011).
73. Zhao, Y., Xiong, X. & Sun, Y. DEPTOR, an mTOR inhibitor, is a physiological substrate of SCF(βTrCP) E3 ubiquitin ligase and regulates survival and autophagy. *Mol. Cell* **44**, 304–316 (2011).
74. Choi, J. H. et al. The FKBP12-rapamycin-associated protein (FRAP) is a CLIP-170 kinase. *EMBO Rep.* **3**, 988–994 (2002).
75. Martínez, O. & Reyes-Valdés, M. H. Defining diversity, specialization, and gene specificity in transcriptomes through information theory. *Proc. Natl Acad. Sci. USA* **105**, 9709–9714 (2008).

Acknowledgements

This work was supported in part by Jubiläumsstiftung von Swiss Life and by the Swiss National Science Foundation grant #CRSII3_160760.

Author contributions

M.A., N.M., and M.Z. conceived the study. D.J.H. handled the mice, D.J.H. and N.M. obtained the samples. N.M., L.T. carried out the experiments. A.S. carried out the mass spectrometry experiments. M.A. analyzed all data with the help of A.G. on mTOR pathway analysis. M.A., N.M., A.G., and M.Z. wrote the manuscript with help from D.J.H., M.A.R., and L.T. Funding was obtained by M.A.R., M.Z., and N.M. All authors have read and approved the manuscript.

Competing interests

The authors declare no competing interests.

Additional information

Supplementary information The online version contains supplementary material available at https://doi.org/10.1038/s42003-024-06679-4.

Correspondence and requests for materials should be addressed to Meric Ataman or Mihaela Zavolan.

Peer review information *Communications Biology* thanks Pei Wang and the other, anonymous, reviewer(s) for their contribution to the peer review of this work. Primary Handling Editors: Joao Valente.